Geomechanics and Engineering, *Vol. 22, No. 2 (2020) 133-142*
DOI: https://doi.org/10.12989/gae.2020.22.2.133

Case study of the mining-induced stress and fracture network evolution in longwall top coal caving

Cong Li[1,2a], Jing Xie*[1,2], Zhiqiang He[1,2a], Guangdi Deng[1,2a], Bengao Yang[1,2a] and Mingqing Yang[1,2a]

[1]State Key Laboratory of Hydraulics and Mountain River Engineering,
College of Water Resource and Hydropower, Sichuan University, Chengdu, 610065, China
[2]MOE Key Laboratory of Deep Underground Science and Engineering, Sichuan University, Chengdu 610065, China

(Received April 9, 2020, Revised May 28, 2020, Accepted June 8, 2020)

Abstract. The evolution of the mining-induced fracture network formed during longwall top coal caving (LTCC) has a great influence on the gas drainage, roof control, top coal recovery ratio and engineering safety of aquifers. To reveal the evolution of the mining-induced stress and fracture network formed during LTCC, the fracture network in front of the working face was observed by borehole video experiments. A discrete element model was established by the universal discrete element code (UDEC) to explore the local stress distribution. The regression relationship between the fractal dimension of the fracture network and mining stress was established. The results revealed the following: (1) The mining disturbance had the most severe impact on the borehole depth range between approximately 10 m and 25 m. (2) The distribution of fractures was related to the lithology and its integrity. The coal seam was mainly microfractures, which formed a complex fracture network. The hard rock stratum was mainly included longitudinal cracks and separated fissures. (3) Through a numerical simulation, the stress distribution in front of the mining face and the development of the fracturing of the overlying rock were obtained. There was a quadratic relationship between the fractal dimension of the fractures and the mining stress. The results obtained herein will provide a reference for engineering projects under similar geological conditions.

Keywords: longwall top coal caving; fracture network; mining-induced stress; fractal dimension; fracture connectivity

1. Introduction

The dynamic evolution of mining-induced fractures has nonignorable effects on safe and efficient mining (Shi *et al*. 2019). Especially under the coupling effect of the mining dynamics and gas pressure, the overlying strata are overlaid with the mining-induced fractures and original fractures, and their temporal and spatial evolution regularity are very complex. Many researches have studied the mechanical properties of rocks and the distribution of mining fractures (Usanov *et al*. 2013, Unver and Yasitli 2006, Beskardes and Weiss 2018).

Numerous studies via numerical simulations have been conducted to investigate the mining-induced stress and fracture network evolution. Yasitli and Unver (2005) studied the distribution of the maximum vertical abutment stresses and the fractured zone. Singh and Singh (2009) proposed a numerical modeling approach for predicting the progressive caving behavior of strata and the performance of a powered roof support. Alehossein and Poulsen (2010) developed a yield and caveability criterion based on *in-situ* conditions in the top coal in advance of the mining face (yield) and behind the supports (caveability).

Extensive field monitoring and laboratory tests have been conducted to study the evolution of the deformation, stress, and fractures in longwall top coal caving (LTCC) (Lata and Zakhmi 2019, Mahdi *et al*. 2019, Wang *et al*. 2019, Lee *et al*. 2019). Smyth and Buckley (1993) explored the feasibility and effectiveness of using a combination of microstratigraphy and statistics. Zhang *et al*. (2015) conducted triaxial tests on coal samples to simulate the three mining methods and found that the mining layout influences the spatial morphology of the mining-induced fractures. Mohammadi (2019) theoretically analyzed the damage process of fractured rock. Jafari and Babadagli (2012) found that fractal characteristics of fracture networks could be used in fracture network mapping and the preparation of permeability data. In addition, the fracture network is related to the distribution characteristics of the stress field. Singh and Singh (2009) proposed an empirical relationship to estimate the range of influence and the value of the ultimate induced stress (vertical) over coal pillars. Gao *et al*. (2013) found that the variation tendency of the fractal dimension and abutment pressure has the same characteristic value by borehole video field monitoring. Therefore, it is necessary to study the evolution of the fracture network and the distribution of the mining stress according to engineering practice.

In this paper, based on field tests of the no. 8309 working face in the Tongxin Coal Mine, the real-time evolution process of the fracture network was studied. The fractal characteristics and connectivity of the fracture network in front of the working face were revealed by using fractal geometry theory and the projection algorithm. The

∗Corresponding author, Ph.D.
E-mail: xiejing200655@163.com
[a]Ph.D. Student

http://www.techno-press.org/?journal=gae&subpage=7 ISSN: 2005-307X (Print), 2092-6219 (Online)

space-time characteristics of the fracture network and its relationship with the advanced abutment pressure were analyzed.

2. Illustration of the mining-induced stress and fracture fields

The fracture network is not only the main fluid passage of the seepage, flow and drainage but also affects the stress distribution characteristics of the coal and rock mass. With the working face moving forward, the mining disturbance changes the stress balance of the *in-situ* rock. The mining stress field causes different degrees of damage to the rock mass, and new cracks are constantly formed. The fracture network tends to be complex and affects the distribution of the mining stress. There should have a correlation between the mining-induced stress and the fracture network.

However, it is difficult to accurately describe large-scale fractures and the distribution of stress. In this paper, the fracture network in front of the working face was recorded by a borehole video instrument. Fractal theory was applied to analyze the time–space characteristics of the fracture network, as well as its relationship with the abutment pressure. The discrete element model established by the universal discrete element code (UDEC) was used to obtain the mining stress field.

3. Field test of the fracture network evolution

3.1 Geological conditions

The test site was located in the no. 8309 working face of the Tongxin Coal Mine, which had a capacity of 5 million tons. The cover depth was approximately 476.3-601.0 m, and the average coal seam thickness was 14.88 m. The coal cutter and caving had mining thicknesses of 3.9 and 10.98 m, respectively. The average dip angle was 1.5°. The field test site is shown in Fig. 1.

3.2 Test scheme

The formation and distribution of mining fissures are very complicated. During the process of mining, a CXK12_Z borehole video instrument (Gao *et al*. 2018) was used to record the fracture evolution of the borehole wall (see Fig.2). The drilling direction was designed to be

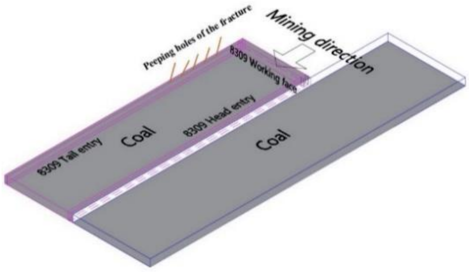

Fig. 1 Field test site

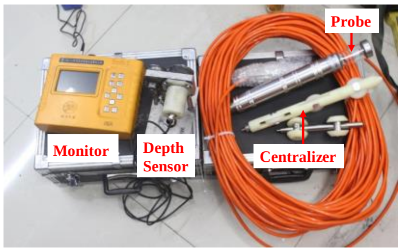

Fig. 2 CXK12_Z borehole video instrument

Table 1 Borehole layout parameters (roadway azimuth 234°)

Borehole ID	Azimuth /°	Dip angle /°	Borehole diameter /mm	Height from floor /m	Depth /m
#1	322	70	65	3.7	26.5
#2	335	65	65	3.7	19.7
#3	330	65	65	3.7	20
#4	341	50	65	3.7	29.2
#5	332	68	65	3.7	27.3

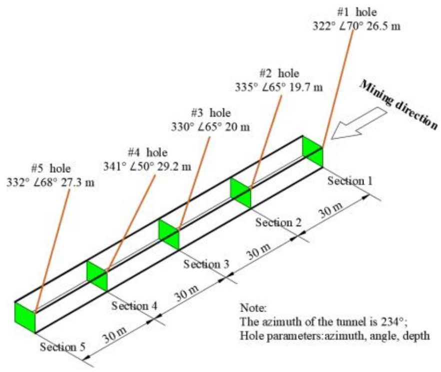

Fig. 3 Schematic diagram of the drilling location

perpendicular to the advance direction and parallel to the working face, and the layout parameters are shown in Fig. 3. The probe was integrated with a three-dimensional compass, which can quantitatively analyse the occurrence, width and location of fractures.

Five boreholes were designed. The borehole layout parameters are shown in Table 1. The space location is shown in Fig. 3. When the probe was 250 m from the mining face, the observation was started. Then, the probe was slowly pushed to the bottom of the borehole, and the crack image was obtained and spliced into a panorama. Two processing methods were used to characterize the fracture network. In the first method, professional postprocessing software was utilized to identify the fractures in the map. The depth, occurrence and width of each fracture were obtained. In the second method, the graph was imported into AutoCAD software, and different width curves were used to trace the cracks with different widths. Through these two processes, the evolution of the fracture network was recorded quantitatively.

3.3 Evolution process of the mining fracture network

After three months of testing, a total of 1552 m

(a) Intact strata (#1 borehole 11.3 m)

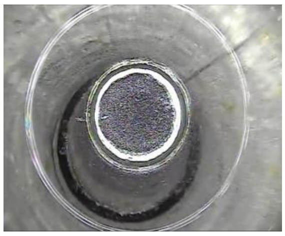

(b) Separation (#5 borehole 27.1 m)

(c) Random fractures (#5 borehole 25.4 m)

(d) Broken zone (#4 borehole 7.5 m)

Fig. 4 Several fracture patterns

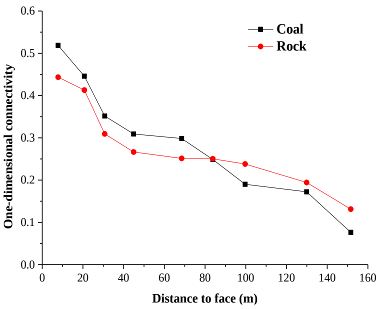

(a) #1 borehole

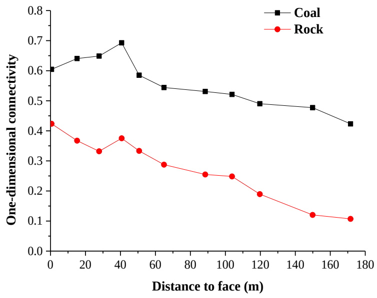

(b) #2 borehole

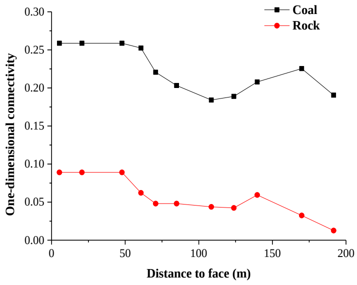

(c) #3 borehole

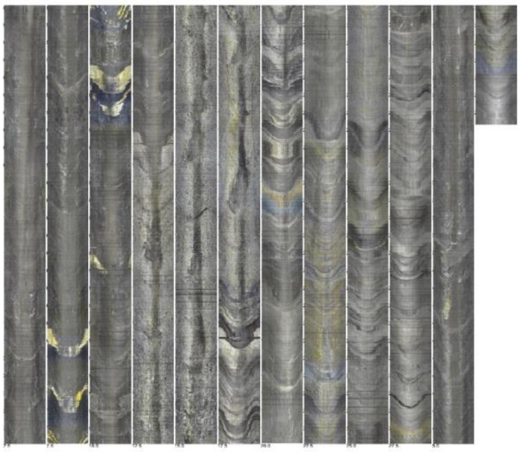

Fig. 5 The panorama of #5 borehole (the distance from the working surface is 21.7 m)

of the borehole wall were obtained. According to the morphological characteristics of the fractures in the

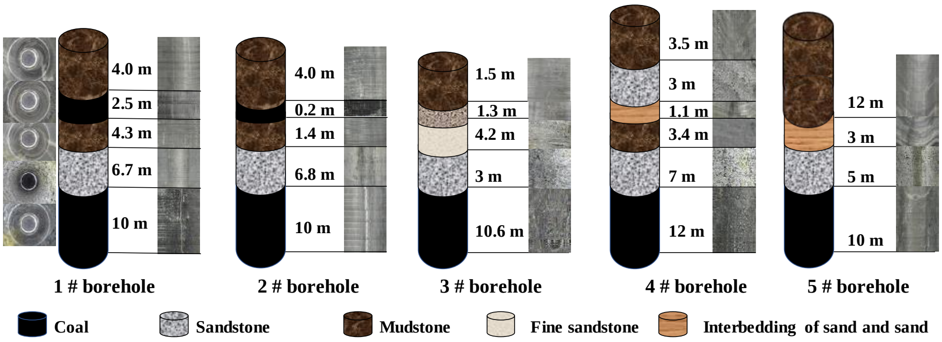

Fig. 6 Borehole histogram

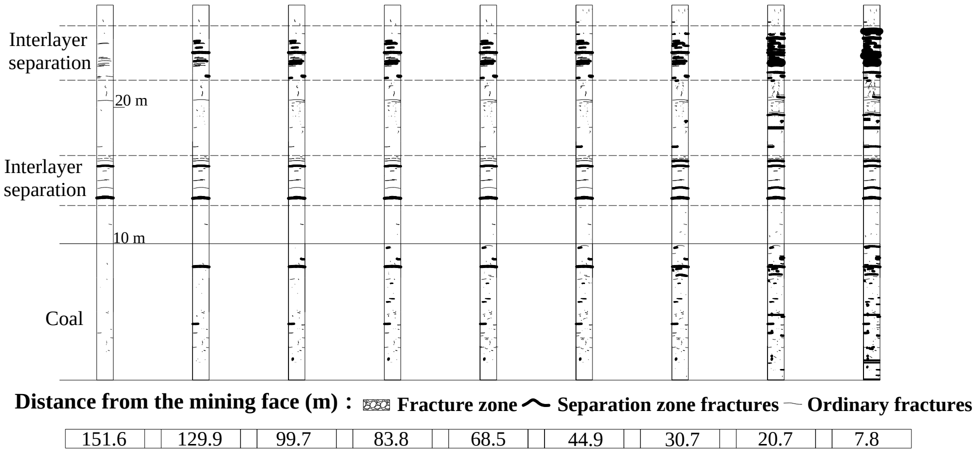

(a) #1 borehole

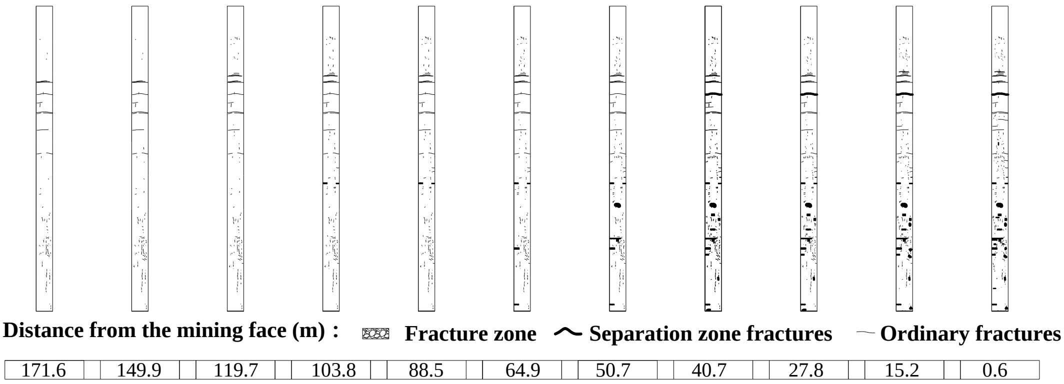

(b) #2 borehole

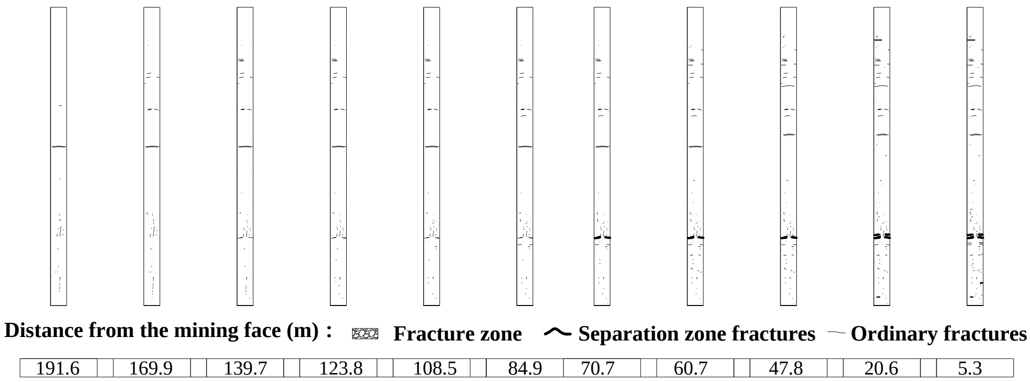

(c) #3 borehole

Fig. 7 Evolution of the crack network for each borehole wall in the roof

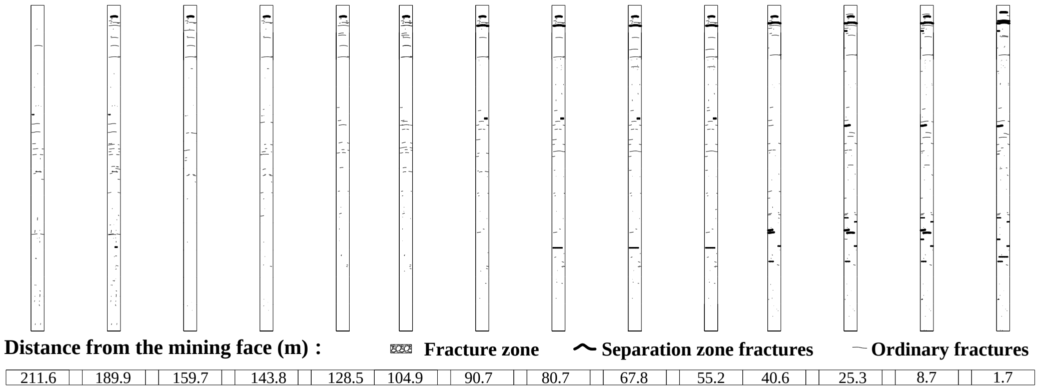

(d) #4 borehole

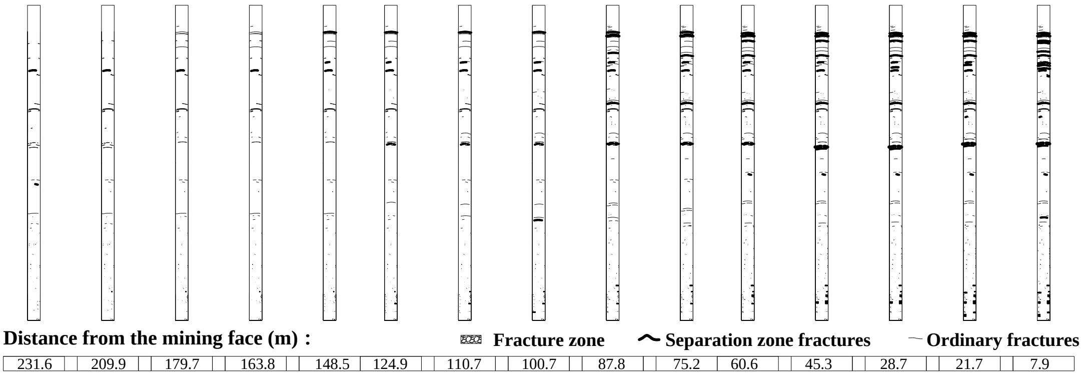

(e) #5 borehole

Fig. 7 Continued

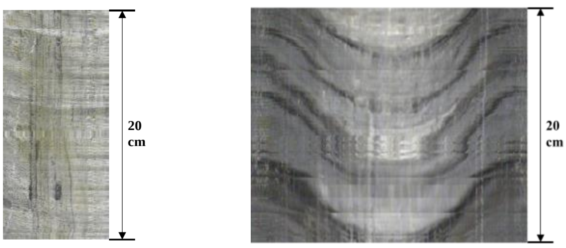

(a) Fractures in the rock strata

(b) Fractures in the coal seam

Fig. 8 Borehole fractures

borehole wall, the cracks can be divided into broken zones, separations and random fractures. The broken zone is a seriously damaged area under the influence of mining, which is mainly distributed in the middle and lower parts of the borehole. The broken zone presents the phenomenon of block breaking and spalling. The separation is a relatively obvious fracture in the borehole, and the width can be clearly observed in the image. Random fractures are common in boreholes with a small width. Fig. 4 and Fig. 5 show several fracture patterns. Fig. 6 shows borehole histogram.

As shown in Fig. 7, the fractures of borehole #1 were mainly concentrated at 10 m (coal-rock boundary) and 25 m (weak zone). The lower part of the #2 - #4 boreholes were dominated by random fractures, while the middle and upper part of the #2 - #4 boreholes had fewer fractures. The initial influence range of mining was more than 100 m.

Overall, the distribution of mining fractures was related to the lithology and its integrity. The weak stratum was dominated by random fractures that developed into broken areas. The sizes of the fractures in the hard rock formations were relatively large, and they were mainly longitudinal fractures and delaminated fractures (see Fig. 8).

With the advancement of the mining face, small cracks were continuously produced in the borehole wall. With the continuous generation of new fractures, the complexity of the fracture network gradually increased and finally evolved into a broken area. In this area, the borehole wall was continuously cut by the initial fractures and mining-induced fractures, and the transfer performance of the stress became weak.

3.4 Evolution of the mining-induced fracture network

The fracture field is the fundamental cause of the damage and instability of the rock mass. The development, evolution and spatial distribution of fractures directly affect the stability of the coal and rock mass. The mining-induced fracture evolution and its fractal characteristics are closely related to the mining disturbance (Daniel and Robert 2019, Daniel *et al*. 2020). Fractal geometry theory and MATLAB software were adopted to analyze the evolution of the mining-induced fracture network. The calculation principle is as follows:

The box dimension can be calculated as Eq. (1) (Gao *et al*. 2013).

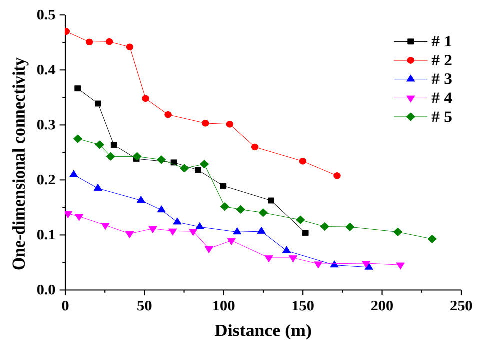

Fig. 9 One-dimensional connectivity of the fracture

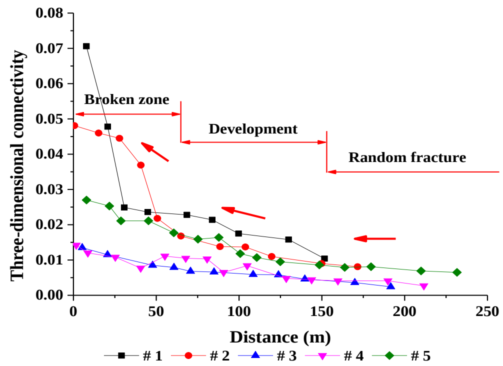

Fig. 10 Three-dimensional connectivity of the fracture

$$D = \lim_{\delta \to 0} \frac{\lg N_\delta(F)}{-\lg(\delta)} \tag{1}$$

where D, δ, F, and $N_\delta(F)$ represent the box dimension, the diameter of the box, a nonempty bounded subset, and the minimum count of the set F covered by the largest diameter, respectively.

There is a direct relationship between the fracture connectivity and fluid seepage (Berkowitz 2002). Therefore, the connectivity can also be used as an index to evaluate the permeability and mobility of gas in coal seams. In this paper, the projection method was used. The method binarized the images of the borehole wall. Then, all the cracks in the image were projected to the hole depth direction, and the number of fracture pixels was calculated. The proportion of the number of fracture pixels along the axial direction of the borehole was defined as the one-dimensional connectivity K_1, which is shown in Eq. (2) (Qiu *et al*. 2016).

$$K_1 = \frac{\sum_{i=1}^{n} N_i}{N} \tag{2}$$

where N_i, n, and N represent the number of single fracture projection pixels, total fractures, and number of pixels along the axial direction of the borehole, respectively. Notably, the number of pixels in the overlapping part of the fractures needs to be deleted in the calculation process.

In addition, the calculated fracture area was equivalent to the side surface area of the cylinder with the diameter of the borehole. Thus, the ratio of the fracture area to the borehole wall area was deduced as the equivalent three-dimensional connectivity K_3, as shown in Eq. (3) (Qiu *et al*. 2016).

$$K_3 = \frac{V'}{V} = \frac{\pi r^2 h'}{\pi r^2 h} = \frac{h'}{h} = \frac{A'}{2\pi r h} = \frac{A'}{A} \tag{3}$$

where V' is the equivalent fracture volume; V is the volume of the borehole; h is the drilling depth; A' is the fracture area; and A is the borehole wall area.

As seen from Fig. 9 and Fig. 10, with the advancing working face, its fractal dimension and connectivity increased continuously. The growth trend of each borehole was similar; they all experienced slow growth, rapid growth and then tended to be stable. The maximum connectivity was less than 0.5, and the fractal dimension was between 0.85-1.34. The growth rate of the connectivity and the initial fracture complexity of the different boreholes were different.

The whole process of 3D connectivity can be roughly divided into three stages. When the distance from the working face was more than 150 m, the fracture growth was slow. When the distance ranged from 50 m-150 m, the rock mass in front of the working face was affected by the mining operation, and the fractal dimension and the one-dimensional connectivity increased approximately linearly.

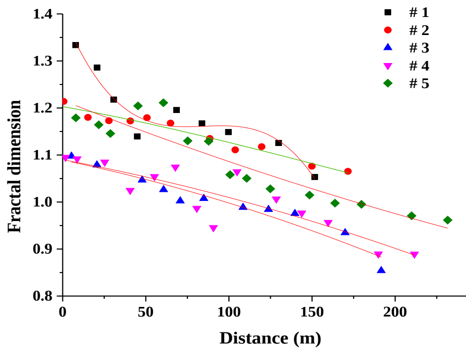

Fig. 11 Real-time fractal dimension of the mining crack boreholes

Table 2 Physico-mechanical parameters of different types of rocks

Rock type	Density (kg/m^3)	Bulk modulus (GPa)	Shear modulus (GPa)	Internal friction angle (°)	Cohesion (MPa)	Tensile strength (MPa)
Overburden strata	2400	18.2	11.45	32	8	2.6
Coal	1590	2.9	1.35	30	2	1
Underlying sandstone	2530	18.2	11.45	32	8	2.6

Table 3 Physico-mechanical parameters of the rock joints

Rock joint	Normal stiffness (GPa)	Shear stiffness (GPa)	Internal friction angle (°)	Cohesion (MPa)
Overburden strata	33.4	8.35	35	8
Coal	4.7	1.2	28	2
Underlying sandstone	33.4	8.35	32	8

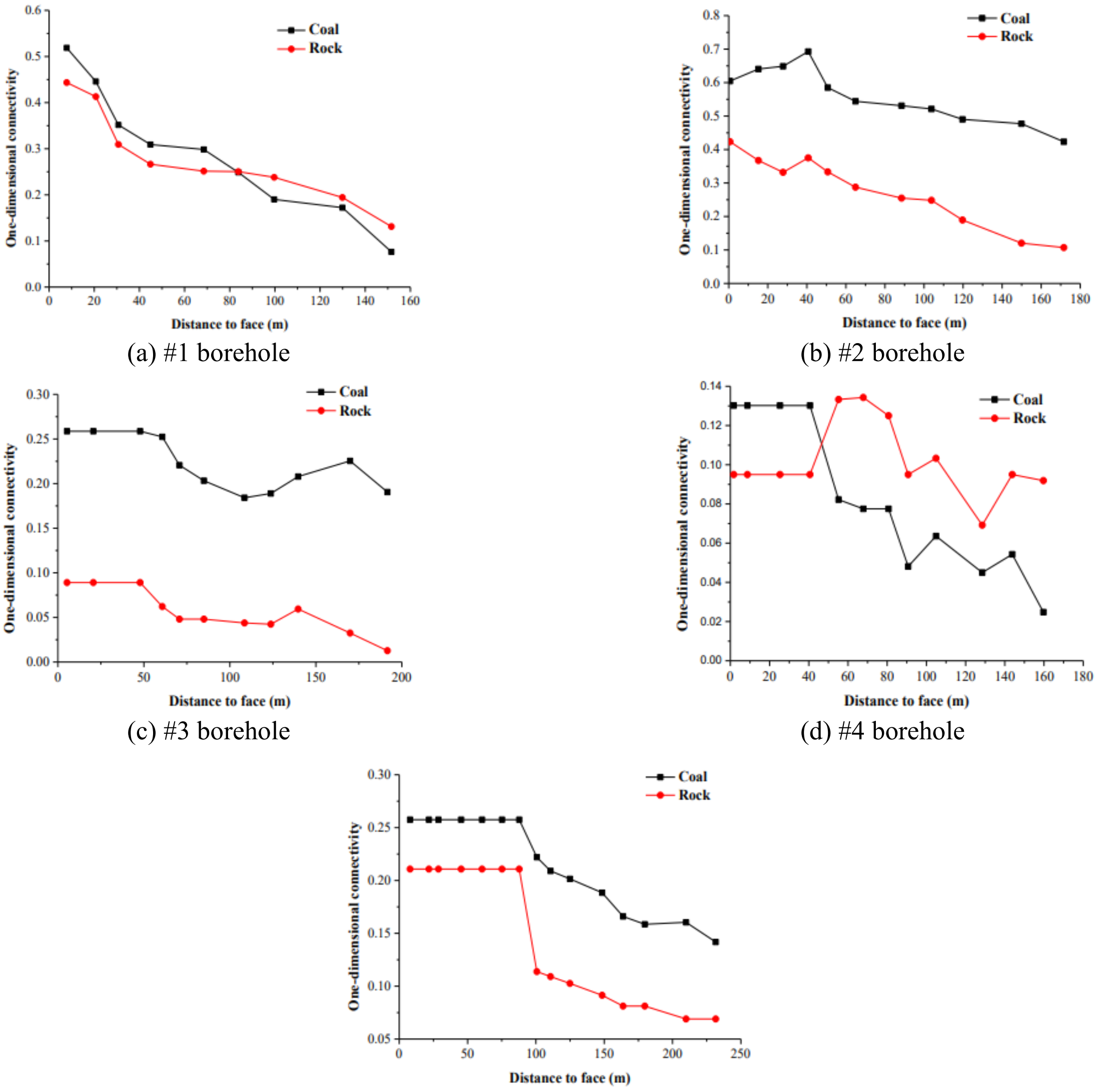

(a) #1 borehole (b) #2 borehole

(c) #3 borehole (d) #4 borehole

(e) #5 borehole

Fig. 12 Fractal dimension of the mining fractures in different strata

When the distance was less than 50 m, the three-dimensional connectivity rate increased rapidly.

Generally, within 50 m from the mining face, the mining-induced influence was strong, and the fracture connectivity and fractal dimension showed a sharp rise, which is a strong disturbance stage. Therefore, the designed advance support distance should be more than 50 m, and the deformation of the surrounding rock should be controlled in advance to reduce the initial damage.

3.5 Characteristics of the fracture evolution in different strata

As seen from Fig. 12, fractures occurred in the coal seam and rock stratum with obvious differences in the growth forms. In the coal seam, there were mainly small fissures that developed and penetrated into large fissures. Instead, there were two types of fractures in the hard rock stratum: longitudinal fractures and separations. The separations were generally located at the top of the borehole and completely intersected with the borehole. Generally, the one-dimensional fracture connectivity in the coal seam was generally higher than that in the rock stratum.

4. Numerical simulation of the mining stress evolution

A numerical model can help to understand the stress distribution in LTCC. In this paper, the discrete element method UDEC was applied to analyze the mining stress field caused by mining.

4.1 Simulation procedures

The discrete element method consists of completely separated elements that allow the finite displacement and rotation of the discrete elements (Krishanu *et al*. 2009). Prefabricated cracks were added to the model. First, the boundary condition was applied, the initial stress of the element was preset, and the initial geo-stress balance was calculated. Then, the step-by-step excavation method was

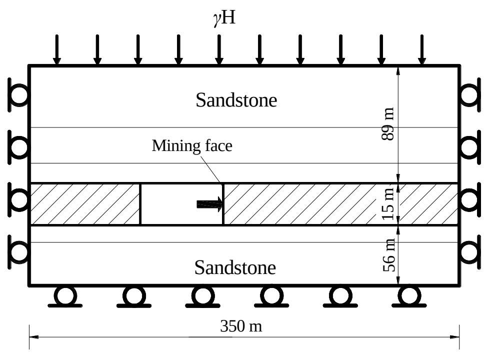

Fig. 13 Schematic diagrams of numerical models for LTCC

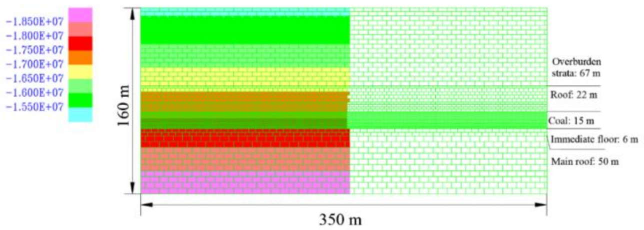

Fig. 14 *In-situ* stress field and block partition

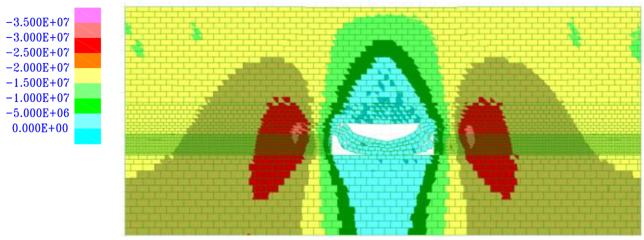

Fig. 15 Stress field distributions for the mining layouts (excavation of 70 m)

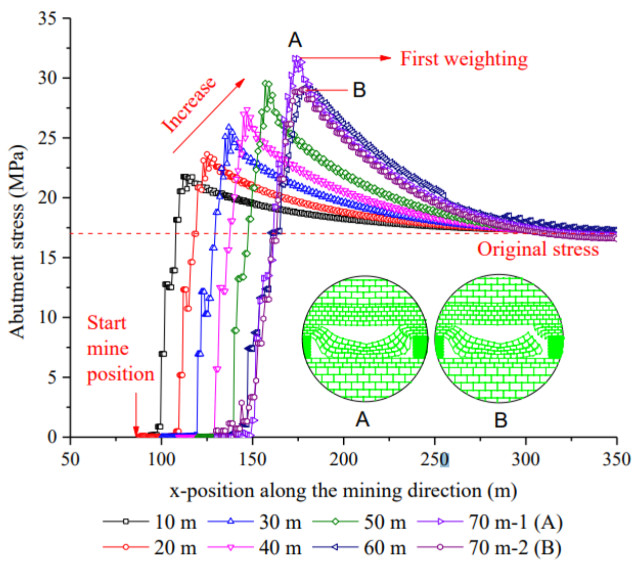

Fig. 16 Abutment stress at different mine lengths

used to simulate the mining process. We excavated 10 m in each step and calculated the stress balance. The monitoring line was designed to record the process of stress evolution during model excavation.

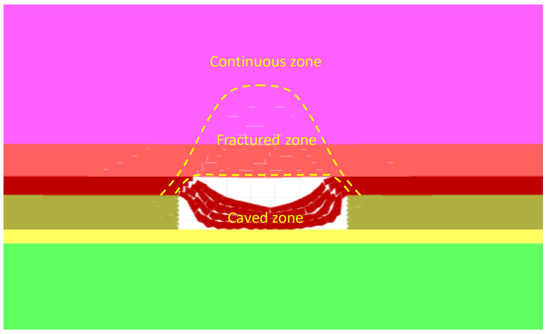

Fig. 17 Simulated caved zone, fractured zone and continuous zone due to the extraction of a panel

4.2 Model establishment

According to the geological conditions of the 8309 working face and considering the boundary effect, a model was established with a length of 350 m and a height of 160 m. The displacement at the bottom of the model was completely constrained. It was assumed that there was only vertical displacement on both sides of the model, and the horizontal displacement was zero. The gravity stress (15.3 MPa) of the overlying strata was applied on the top of the model to simulate the depth. The Mohr-Coulomb failure criterion was used in the numerical model, and the surface contact Coulomb slip model was applied in the joint model. The material parameters refer to the research literature (Li *et al*. 2018, Yu *et al*. 2015) of the similar mining area, as shown in Tables 2-3. The division of the elements and geo-stress balance are shown in Figs. 13 and 14.

4.3 Numerical simulation results

From the stress analysis, Fig. 15 shows the stress distribution during the initial collapse. Fig. 16 shows the distribution of the abutment pressure with mining distances of 10 m, 20 m, 30 m, 40 m, 50 m, 60 m and 70 m. The stress fluctuation was complex and rapid. The stress near the mining face was almost 0 MPa. At 10-30 m from the mining face, the stress quickly increases to the peak. Subsequently, the stress gradually decreased to the original rock stress of 17 MPa. When the excavation was 70 m, the maximum peak stress was 31.6 MPa, and the roof began to collapse for the first time. As shown in Fig. 16, 70 cm^{-1} is the stress before collapse, and 70 m^{-2} represents the state after the collapse. After the roof collapsed, the peak stress was significantly reduced to 29 MPa. The abutment pressure of fully mechanized LTCC had a wide influence.

At the initial stage of excavation, the immediate roof was in a fixed state, so there were few cracks. No collapse (or a collapse) was observed at this stage, and the roof remained stable. With the advance of the working face, the roof began to bend, break and extend deeper. When the mining length was 70 m, the fracture height was approximately 34 m. Due to the hard roof, strong joint strength and horizontal force, a large area of the suspended roof was formed, resulting in a high abutment pressure. The model can capture three different regions, namely, the caved zone, fractured zone and continuous zone, as shown in Fig. 17.

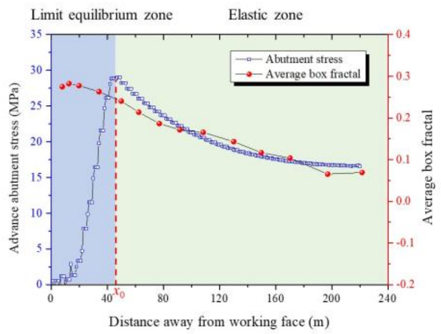

Fig. 18 Advanced abutment pressure and fracture fractal dimension

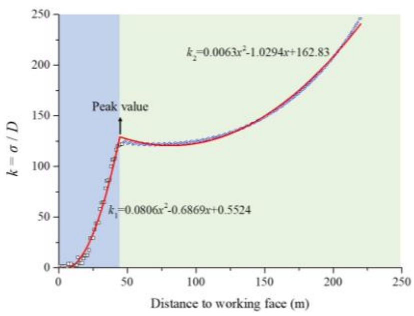

Fig. 19 The quadratic fitting curve

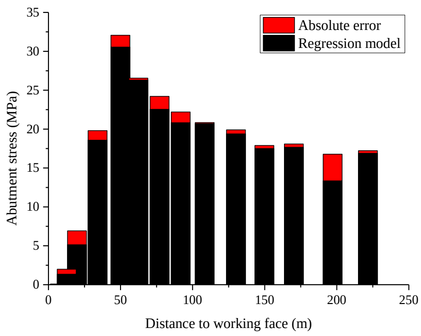

Fig. 20 Error of the regression model

5. Discussion

There is a relationship between the fractal dimension of the fracture and abutment pressure. As shown in Fig. 18, the variation trend of the advanced abutment pressure was basically consistent with that of the fractal dimension of the fracture network. Taking the peak abutment pressure as the boundary, the abutment pressure was divided into two stages: elastic zone and limit equilibrium zone. In the elastic zone, the vertical pressure had not yet reached the compressive strength. The fracture was mainly a random fracture, and the fractal dimension curve grew slowly. In the limit equilibrium zone, the rock mass was basically broken. After the peak value, the fracture area became larger, and the fractal dimension increased to a maximum value. Gao *et al*. (2013) found that the fractal dimension of a fracture network can be used to quantitatively evaluate the spatiotemporal evolution of the abutment pressure $\sigma_1 \propto kD$.

In this paper, based on the experimental results, the relationship between the fractal dimension and abutment pressure was approximately quadratic. That is,

$$\sigma_1 \propto \begin{cases} k_1(x)D & x < x_0 \\ k_2(x)D & x > x_0 \end{cases} \tag{4}$$

The quadratic fitting curve is drawn, as shown in Fig. 19. Fig. 20 shows the model error. It can be seen that the fitting error is small.

6. Conclusions

The findings of this study are as follows:

- The fractures are mainly concentrated at depths of 10 m and 25 m. When the distance from the working face is more than 150 m, it can be defined as an undisturbed zone. The zone with a distance of 50-150 m from the working face can be defined as a weak disturbance region. Within 50 m of the working face, it can be defined as a strong disturbance zone.
- Affected by mining, the fracture network changes from simple to complex. The characteristics of the fracture network in different strata are different. In the coal seam, there are mainly small fissures that develop and penetrate into large fissures. In the hard rock stratum, the longitudinal fractures and separations are dominant. The development of coal seam fractures is generally greater than that of the rock stratum.
- Through numerical simulation, the distribution of the abutment pressure in front of the working face and the development of overlying rock fracture are obtained, and they are in accordance with the quadratic relationship.

Acknowledgments

This study was financially supported by the China Postdoctoral Science Foundation (Grant No. 2019M653403).

References

Alehossein, H. and Poulsen B.A. (2010), “Stress analysis of longwall top coal caving”, *Int. J. Rock Mech. Min. Sci.*, **47**(1), 30-41. http://doi.org/10.1016/j.ijrmms.2009.07.004.

Ashtari, M., Mousavi, S.E., Cheshomi, A. and Khamechian, M. (2019), “Evaluation of the single compressive strength test in estimating uniaxial compressive and Brazilian tensile strengths and elastic modulus of marlstone”, *Eng. Geol.*, **248**, 256-266. https://doi.org/10.1016/j.enggeo.2018.12.005.

Berkowitz, B. (2002), “Characterizing flow and transport in fractured geological media: A review”, *Adv. Water Resour.*, **25**(8), 861-884. http://doi.org/10.1016/S0309-1708(02)00042-8.

Beskardes, G.D. and Weiss, C. (2018), “Modelling dc responses of 3-D complex fracture networks”, *Geophys. J. Int.*, **214**, 1901-1912. http://doi.org/10.1093/gji/ggy234.

Daniel, B. and Robert, J. (2019), “Experimental study on models of cylindrical steel tanks under mining tremors and moderate earthquakes”, *Earthq. Struct.*, **17**(2), 175-189.

https://doi.org/10.12989/eas.2019.17.2.175.

Daniel, B., Michal, W. and Robert, J. (2020), "Numerical investigation on behaviour of cylindrical steel tanks during mining tremors and moderate earthquakes", *Earthq. Struct.*, **18**(1), 97-111. https://doi.org/10.12989/eas.2020.18.1.097.

Gao, M.Z., Jin, W.C., Dai, Z.X. and Xie, J. (2013), "Relevance between abutment pressure and fractal dimension of crack network induced by mining", *Int. J. Min. Sci. Technol.*, **23**(6), 925-930. http://doi.org/10.1016/j.ijmst.2013.11.008.

Gao, M.Z., Zhang, R., Xie, J., Peng, G.Y., Yu, B. and Ranjith, P.G. (2018), "Field experiments on fracture evolution and correlations between connectivity and abutment pressure under top coal caving conditions", *Int. J. Rock Mech. Min. Sci.*, **111**, 84-93. http://doi.org/10.1016/j.ijrmms.2018.01.003.

Jafari, A. and Babadagli, T. (2012), "Estimation of equivalent fracture network permeability using fractal and statistical network properties", *J. Petrol. Sci. Eng.*, **92-93**, 110-123. http://doi.org/10.1016/j.petrol.2012.06.007.

Krishanu, R., Hieng, H.L. and James, B.P.L. (2019), "Finite element modelling of back-to-back built-up cold-formed stainless-steel lipped channels under axial compression", *Steel Compos. Struct.*, **33**(1), 37-66. https://doi.org/10.12989/scs.2019.33.1.037.

Lata, P. and Himanshi, Z. (2019), "Fractional order generalized thermoelastic study in orthotropic medium of type GN-III", *Geomech. Eng.*, **19**(4), 295-305. http://doi.org/10.12989/gae.2019.19.4.295.

Lee, C., Nam, H., Lee, W., Choo, H. and Ku, T. (2019), "Estimating UCS of cement-grouted sand using characteristics of sand and UCS of pure grout", *Geomech. Eng.*, **19**(4), 343-352. http://doi.org/10.12989/gae.2019.19.4.343.

Li, S., Gao, M., Yang, X., Zhang, R., Ren, L., Zhang, Z., Li, G., Zhang, Z. and Xie, J. (2018), "Numerical simulation of spatial distributions of mining-induced stress and fracture fields for three coal mining layouts", *J. Rock Mech. Geotech. Eng.*, **10**(5). http://doi.org/10.1016/j.jrmge.2018.02.008.

Mohammadi, H. and Pietruszczak, S. (2019), "Description of damage process in fractured rocks", *Int. J. Rock Mech. Min. Sci.*, **113**, 295-302. http://doi.org/10.1016/j.ijrmms.2018.12.003.

Qiu, Z.Q., Gao, M.Z., Lv, Y.C., Wang, M., Xie, J., Xu, X.L. and Zhang, Z.P. (2016), "New calculation method for drilling three-dimensional connectivity rate and its engineering application", *Safety Coal Mines*, **47**(10), 44-47. http://doi.org/10.3321/j.issn:1000-6915.2005.15.003.

Shi, L.Q., Xu, D.L., Wang, Y., Qiu, M. and Hao, J. (2019), "A novel conceptual model of fracture evolution patterns in the overlying strata during horizontal coal seam mining", *Arab. J. Geosci.*, **12**(10), 1-9. http://doi.org/10.1007/s12517-019-4486-x.

Singh, G.S.P. and Singh, U.K. (2009), "A numerical modeling approach for assessment of progressive caving of strata and performance of hydraulic powered support in longwall workings", *Comput. Geotech.*, **36**(7), 1142-1156. http://doi.org/10.1016/j.compgeo.2009.05.001.

Smyth, M. and Buckley, M.J. (1993), "Statistical analysis of the microlithotype sequences in the Bulli Seam, Australia, and relevance to permeability for coal gas", *Int. J. Coal Geol.*, **22**(3-4), 167-187. http://doi.org/10.1016/0166-5162(93)90025-6.

Unver, B. and Yasitli, N.E. (2006), "Modelling of strata movement with a special reference to caving mechanism in thick seam coal mining", *Int. J. Coal Geol.*, **66**(4), 227-252. http://doi.org/10.1016/j.coal.2005.05.008.

Usanov, S.V., Mel'Nik, V.V. and Zamyatin, A.L. (2013), "Monitoring rock mass transformation under induced movements", *J. Min. Sci.*, **49**(6), 913-918. http://doi.org/10.1134/S1062739149060105.

Wang, C., Zhang, N.C., Han, Y.F., Xiong, Z.Q. and Qian, D.Y. (2013), "Experiment research on overburden mining-induced fracture evolution and its fractal characteristics in ascending mining", *Arab. J. Geosci.*, **8**(1), 13-21. http://doi.org/10.1007/s12517-013-1178-9.

Yasitli, N.E. and Unver, B. (2005), "3D numerical modeling of longwall mining with top-coal caving", *Int. J. Rock Mech. Min. Sci.*, **42**(2), 219-235. http://doi.org/10.1016/j.ijrmms.2004.08.007.

Yu, B., Zhang, R., Gao, M.Z., Li, G., Zhang, Z.T. and Liu, Q.Y. (2015), "Numerical approach to the top coal caving process under different coal seam thicknesses", *Therm. Sci.*, **19**(4), 1423-1428. http://doi.org/10.2298/TSCI1504423Y.

Zhang, R., Ai T., Zhou, H.W., Ju, Y. and Zhang, Z.T. (2015), "Fractal and volume characteristics of 3D mining-induced fractures under typical mining layouts", *Environ. Earth Sci.*, **73**(10), 6069-6080. http://doi.org/10.1007/s12665-015-4376-9.

CC